Experimental and Numerical Investigation for Optimum Design of Hydraulic Steel Gates

B.H. MOHAMED[1*], A.M. ANWAR[1], H.H. ELTOBGY[2], G. HELMY[2]

1 Construction Research Institute, National Water Research Center

2 Faculty of Engineering, Benha University, Shoubra

*Corresponding author's email: basma_elbably@nwrc.gov.eg

Abstract- **Steel gates are commonly used in hydraulic structures due to their excellent mechanical properties, particularly in handling hydrostatic pressure. It's important to consider maintenance and operational costs when evaluating their feasibility. This research involved the experimental examination of three prototype steel gates, all sharing the same dimensions of 1.0 m in width and 1.25 m in height. The first gate is a conventional design made from skin steel plates and stiffened with steel channels, serving as a baseline for comparison. The second gate features a thicker steel plate without stiffeners, while the third gate presents an innovative design with two skin plates reinforced by a latticed internal core. Each gate was subjected to equivalent hydrostatic pressure, and their flexural performance was analyzed.**

A Finite Element (FE) model was created using ABAQUS software and validated against the experimental findings, showing a strong correlation between synthetic and experimental results. Additionally, a parametric study was conducted, exploring the performance of a larger gate sized 4.0 m by 4.0 m. The study found that the internally stiffened latticed gates performed the best, achieving the highest load capacity with a 22% reduction in mass compared to the traditional gate design.

 Keywords hydraulic gates; hydrostatic pressure; latticed system; FE.

I.   INTRODUCTION

Hydraulic gates are vital components in hydraulic structures. Their types along with their optimum design can influence the structural and hydraulic performance of the whole structure. The hydraulic gates can be used with different water structures such as barrages, spillways, and navigation locks [1]. In the design of hydraulic gates, some considerations should be taken into account such as; sustainability, leakage prevention, ease of operation, and maintenance…etc. [2]. Different structural systems of gates have been used to resist the applied hydrostatic pressure. Sluice gates, radial gates, sector gates, and miter gates are among these types [3]. The selection of the type of hydraulic gates depends on cost, reliability, navigation, maintenance, and environmental aspects [4]. There are many studies performed on different steel hydraulic gates. Chen and USACE, [5] and [6] stated the different types of hydraulic gates, the main component of each type, the different applied loads, and design considerations. Jaiswal [7] studied the design of the hydraulic gates for hydropower planets and made an optimized design using ANSYS Finite element. Dexter et al. [8] expressed some features of the fatigue and fracture cracks in the hydraulic gates. In addition, Daniel [9] made an overview of the effect of fatigue load on the hydraulic gates and the conditions that should be considered in the design. Liu et al. [10] addressed the importance of considering the hydrodynamic lifting force on hydraulic gates. Gates stiffened with cross girders placed at unequal distances are commonly considered a typical statical system of the gate. This design is followed in most applications regardless of their size and applied loads. This could consequently lead to a tangible increase in the gate mass with a corresponding increase in their operational cost. A suitable alternative was the use of a honeycomb system [11]. This structural system is characterized by its relatively lightweight and high flexural rigidity. [12]. Traditionally, this system is widely used in automotive, aerospace, marine, and aviation industries [13]. The system is typically composed of an upper skin plate and, a lower skin plate, filled with a honeycomb core. [14] and [15]. The in-between core increases the bending and shear stiffness while maintaining the light mass structure [16] and [17]. Baumgart et al. [18] implemented experiments and numerical studies to determine the compressive properties of different shapes of steel honeycomb cores with different thicknesses to ensure their good performance of the system, and there were slight variations between numerical and experimental data of square-celled honeycomb structures in the carried out model validation, the model's use is validated to effectively depict the trends of both in and out-of-plane capacity. Additionally, the honeycomb system was also utilized in the design of bridges' decks. Camata and Shing [19] studied the use of honeycomb decks in bridges under static and fatigue loads. Ghongade et al. [20] performed an experimental and numerical study for a steel honeycomb structure with a circular core

under axial compression behavior. Javanmardi et al. [21] presented a hexagonal honeycomb steel damper as another application of honeycomb structures. The study showed that they have a good range of ductility and high-energy dissipation capability. Similar to honeycomb is the use of latticed systems. Monteiro [22] investigated the effect of the lattice topology on the flexural behavior of sandwich panels, both experimentally and numerically. All the latticed topologies assured maximum stiffness and high energy absorption. Similar to the manufacture of the honeycomb system; Bernardo [23] stated the manufacturing performance of latticed structures: Traditional manufacturing, and Novel manufacturing processes. The traditional manufacturing process is used when the sheet is corrugated and staked together to form a lattice shape. In this technique, there are two different ways used in the corrugation process of the latticed core: the corrugation process, and the expansion process. For novel manufacturing processes, this method is used with materials that could not be processed by the previously described methods, and irregular structures. In this research, the traditional manufacturing process was used in the fabrication of the latticed gate. In the current research, insight into optimizing the design of steel gates by using an internal latticed shape core was made. The new system is like a honeycomb system but with a rhombus-shaped latticed core. Different combinations of steel gates were studied. Three configurations were experimentally and numerically investigated. A further parametric study was conducted numerically by changing the core spacing and thicknesses. The change in the total gate mass and its flexural rigidity were put into a glance and compared for each gate configuration. The gates mainly represent the conventionally plain gates with/without horizontal girders as well as the newly latticed core system gates. Moreover, the feasibility of using the new system was investigated numerically in designing large gates

II.   Materials and Methods

A.   Steel used for gate fabrication

In the current research, physical steel gates were prepared. All steel gates were fabricated using steel grades (52, and 36). The ultimate strength, yield stress, Poisson's ratio, and modulus of elasticity were 520, 360, 0.3, and 1.96E+05 MPa, respectively. The results were obtained through an experimental study conducted in earlier research [24]. Preliminary design for the gates was conducted following the Egyptian Code of Practice for Steel Construction and Bridges, Allowable Stress Design (ASD) [25].
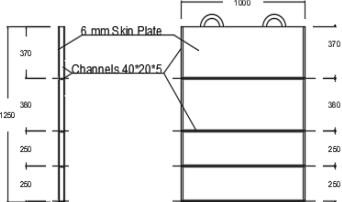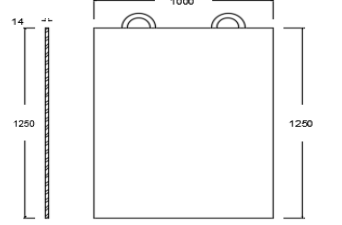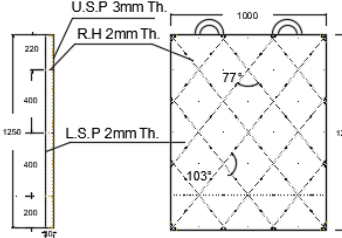
III.   Experimental Program

A.   Gates' Preparation

Three prototype hydraulic gates were prepared for experimental investigation. Table 1 shows a summary of these gates. All gates' dimensions were (1000 x 1250 mm). The thickness was changed as per the preliminary design of each gate. All gates were examined in flexure with a gauge length of 950 mm.

The first gate is the traditional one (TG), which was prepared using a 6 mm skin plate-facing waterside – and stiffened by horizontal steel channels (C40) welded at unequal distances according to the preliminary design. The second, (PG14) plain gate, represents the simplest hydraulic gate that consists only of a plain unstiffened steel plate of 14 mm thickness. The third steel gate (LG30) was a latticed core designed using a 3mm upper skin plate – facing upstream hydrostatic pressure – and a 2 mm lower skin plate. The spacing between the two skin plates was filled with 2 mm strips that were arranged in a rhombus-like vertical stiffener. The lattice core was welded with both the upper and lower skin plates. The whole thickness of the gate was 30 mm.

Table 1. Summary of Examined Gates

Prototype ID	Description	Gates Prototype
TG	Traditional Steel Gate, Skin plate 6mm with Channels 40mm*20mm *5mm main & edge beams (Mass = 79 Kg)	
PG14	Plain Steel Plate (Th. 14 mm) H = 1250 mm, W = 1000 mm (Mass = 137 Kg)	
LG30	Latticed Core Gate (Th. 30 mm) Upper layer (3 mm) –Lower Layer (2mm)- rhumbas stiffeners (2 mm) (Mass = 56 Kg)	

B.   Flexure Test Setup

In this section, a description of the flexure test procedure was explored. All gates were placed horizontally and were simply supported over a gauge length of 950 mm. The gates were loaded using a rigid beam placed along their mid-spans. In such a way, the gates were examined in a one-way flexural mode similar to the actual applied loads on the gates during operation. To simulate the equivalent effect of the applied hydrostatic pressure, the loading beam was exposed to a concentrated load at the lower one-third of the gate's depth. All gates were first loaded up to 5 times the equivalent hydrostatic pressure. This load was sufficient to compare the behavior of the gates at the maximum probable applied load. Figure 1 shows the test setup. The applied load was developed using a manual hydraulic jack. The applied load was measured by an available load cell while three linear variable displacement transducers (LVDTs) were used to measure the deflection. Two transducers were placed at supports while the third was kept at the mid-span of the specimen. The strain was measured using a strain gauge of length 60 mm for all gates. The gauges were pasted on the soffit of each prototype gate at its mid-span and directly beneath the concentration load.

Figure 2. Three points loading flexure test setup

IV. Results and Discussion

A. Flexure Performance

Load-deflection and Load-Strain curves were expressed for the tested gates. Figure 2 shows Load-Deflection curves for all gates and their corresponding Load-Strain plots for the same gates. The performance of the gates was compared, and the corresponding deflection was determined. The best performance was achieved for LG30 where the deflection was reduced by 5 times, and 6.5 times the deflection of PG14 and TG, respectively. This could be attributed to the high flexural rigidity of LG30 due to the continuous latticed core system
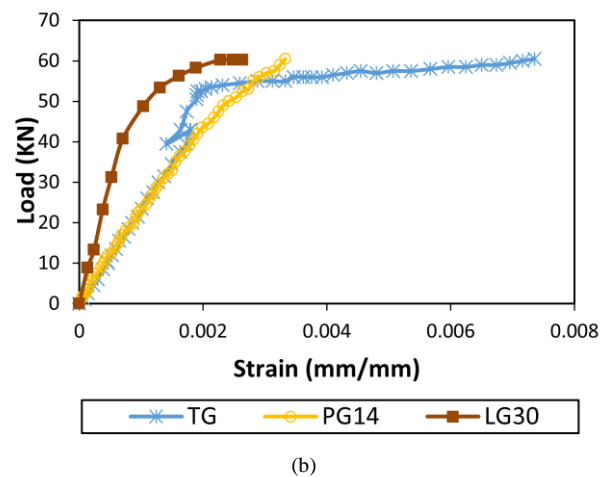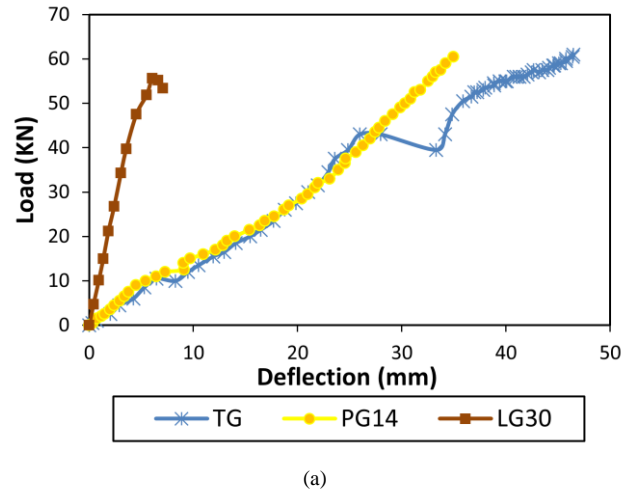

(a)

(b)

Figure 1. (a) Load-Deflection, and (b) Load-Strain curves for examined gates

binding the upper and lower skin plates. The same attitude was observed when comparing the measured strain values for all specimens. At the highest load, the maximum strain of LG30 was reduced by 21% and 63% of the corresponding values of PG14 & TG, respectively. The noticed achievement in the flexure rigidity of LG30 indicated promising behavior of the proposed new system while maintaining the gate mass. It was noticed that the mass of LG30 was around 30%, and 60% less than TG, and PG14, respectively.

B. Failure Modes

This section outlines the failure modes observed in all tested gates. Loading continued until failure occurred at each gate. Plastic deformation due to bending was primarily concentrated in the lower third of the gates, attributed to the linear distribu-

tion of the applied load. Steel yielding began once the elastic load limits were exceeded, following typical behavior. The greatest deformations were observed at the lowest points of the gates.

V. Numerical Modelling

A. Analytical Model Description
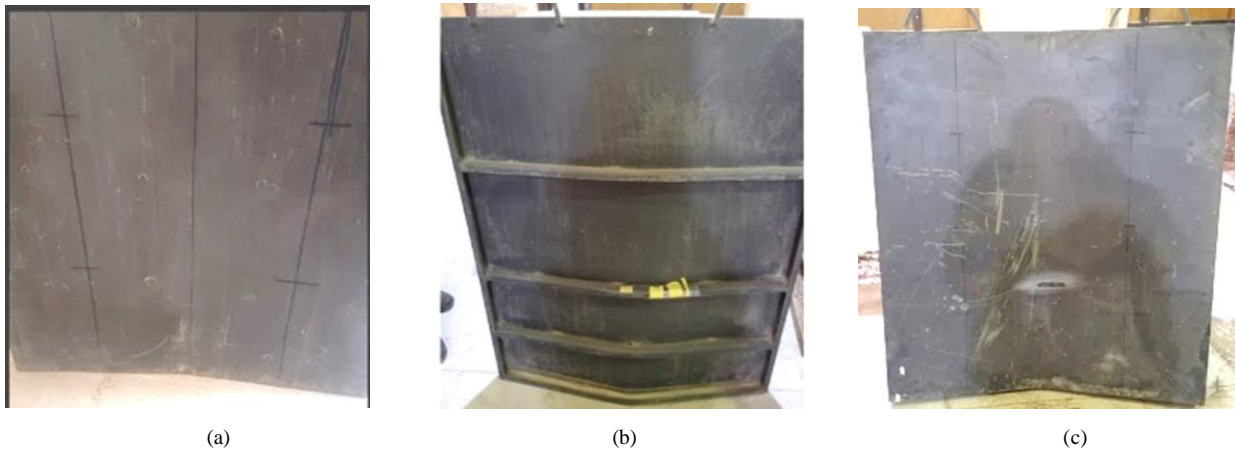
The nonlinear finite element software ABAQUS was utilized

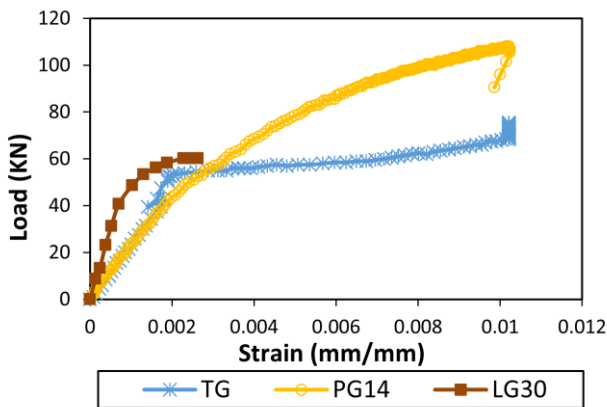Figure 4. Plastic bending deformation for; (a) LG30, (b) TG, and (c) PG14 gates

Figure 3. Complete Load-Strain curves for examined gates

Failure Observations:

LG30: Experienced premature failure due to welding imperfections. Stress concentration at the point of applied load caused localized tearing in the weld, leading to early failure.

TG (Typical Gate): Displayed global distortion, particularly in the skin plate and main beams.

PG14: Significant bending distortions were noted in the lower third of the gate.

Figures 3 and 4 illustrate the failure shapes of the gates and present a complete load-strain plot for all gates up to failure.

for the numerical simulations of the gates. The gates TG, PG14, and LG30 were designated as TG-N, PG14-N, and LG30-N, respectively, for the simulations. To enhance modeling accuracy, 3D 8-node reduced integration solid elements were employed for the TG-N and PG14-N gates, while a deformable 3D 4-node doubly thin curved shell element was used for LG30-N. Reduced integration was applied to account for the lower-order rigidity of the unit, while distributed loads and the mass matrix were determined through full integration. This choice of elements improved calculation efficiency and yielded more accurate stress fields and displacements.

The material model in the analysis was a nonlinear isotropic material. The linear elastic portion of the material's stress-strain curve was defined directly based on properties outlined in Section 2.1. However, the non-linear behavior of the steel required actual stress versus plastic strain data. The engineering plastic strain was derived from the true stress-strain relationship as per Faridmehr et al.

A fine mesh was implemented to improve accuracy and facilitate the identification of crack initiation points. All specimens were equally meshed, with a 20 mm x 20 mm grid in the X and Y directions, and 2 mm thick elements along the Z-direction. Figure 5 illustrates the meshing used for all gates.

The gates were supported by two cylindrical elements with a 20 mm diameter, positioned 50 mm from each edge, and were restrained from movement in all directions. Figure 6 depicts the test setup and boundary conditions for the synthetic gates. Consistent with the experimental approach, hydrostatic pres-

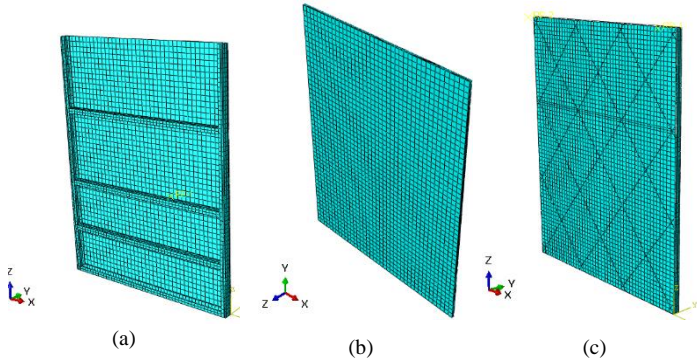sure was applied as a linear uniform load, incrementally increasing until failure.

Figure 5. Meshing of gates; (a) TG-N, (b) PG14-N, and (c) LG30-N
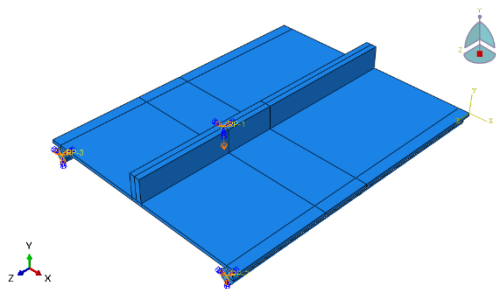

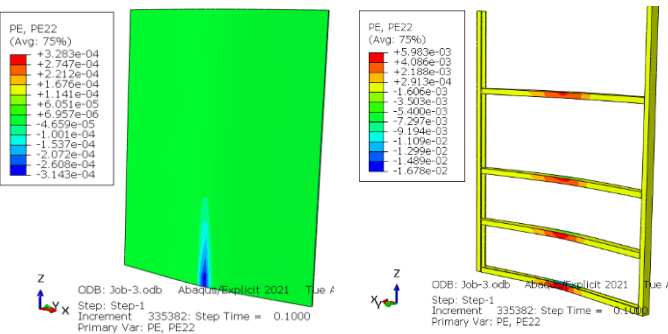Figure 6. Loading configuration of gates showing boundary conditions

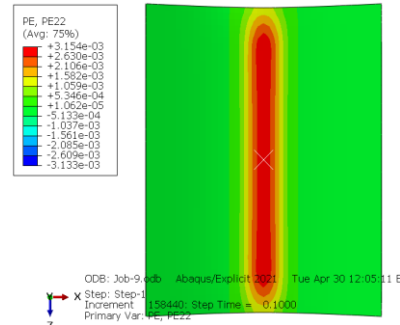Figure 7. Plastic strain (mm/mm) in skin plate and X-Girders of TG-N

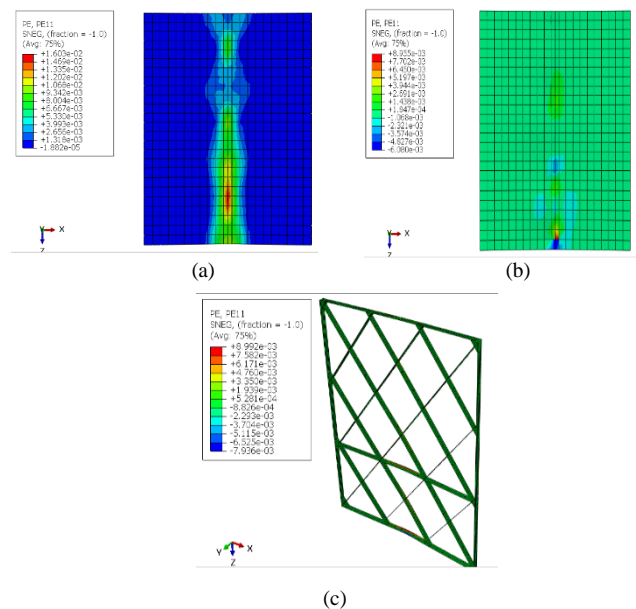Figure 8. Plastic strain (mm/mm) in the middle of PG14 & PG14-N

Figure 9. Plastic strain (mm/mm); (a) Lower Skin Plate, (b) Upper Skin Plate, and (c) Latticed Core of LG30-N

B. Results of Numerical Work

For TG-N, the synthetic model demonstrated flexural performance consistent with the experimental results. As shown in Figure 7, bending distortions occurred in both the crossbeams and the skin plate. The maximum normal stress recorded in the X-direction was 464 N/mm², corresponding to a maximum strain of 0.0291 (mm/mm). The maximum load at failure reached 70 KN, with a displacement of 53 mm.

In the case of PG14-N, the numerical model indicated a maximum normal stress of 371 N/mm² in the X-direction, with a maximum strain of 0.00787 (mm/mm). The peak failure load was 106 KN, accompanied by a displacement of 72 mm, as illustrated in Figure 8. Notably, plastic bending distortions were observed along the mid-span of the gate.

For LG30-N, the maximum normal stress recorded in the X-direction was 196 N/mm² at the soffit of the gate, with a corresponding plastic strain of 0.00163 (mm/mm). In this specimen, strain increased slightly as the loading decreased. The peak failure load reached 82 KN, resulting in a deflection of 15 mm. The failure in the newly designed latticed configuration began with distortions in both the upper and lower skin plates, followed by plastic deformations in the latticed core, as illustrated in Figure 9. The Load-Deflection and Load-Strain curves from both the numerical and experimental studies for all gates are presented in Figures 10, 11, and 12.
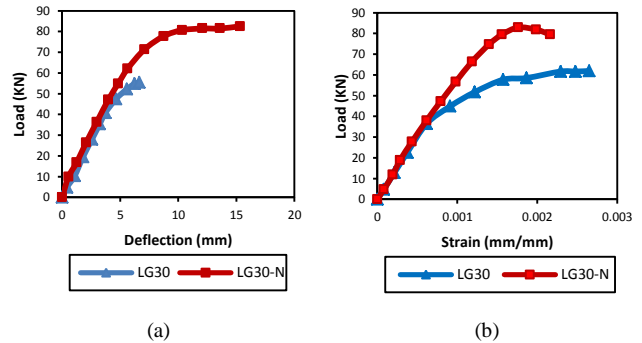

(a)   (b)

Figure 12. (a) Load-Deflection and (b) Load-Strain plots for LG30 and LG30-N

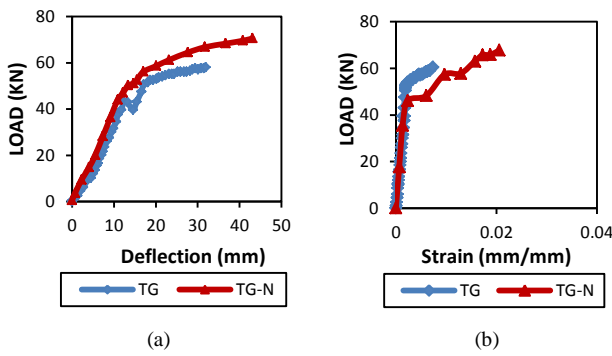(a)   (b)

Figure 10. (a) Load-Deflection & (b) Load-Strain plots for TG & TG-N
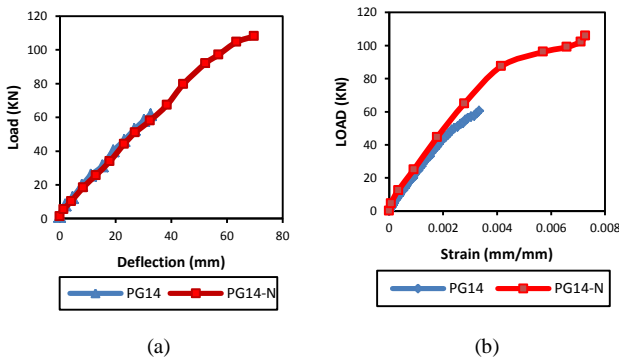

(a)   (b)

Figure 11. (a) Load-Deflection & (b) Load-Strain plots for PG14 and PG14-N

VI.   *Parametric Study*

A.   *Model Description*

The advantages of using lattice sandwich structures in hydraulic gate construction were confirmed through parametric analysis. This section investigates how lattice core dimensions and skin plate thickness affect performance, focusing on gates with dimensions of 1000 mm x 1250 mm. Two groups of latticed core steel gates were analyzed: Group 1 (G1) featured internal lattice dimensions of 256 mm, while Group 2 (G2) had a smaller spacing of 160 mm. For each group, the lattice core thickness was varied between 2 mm and 3 mm, and skin plate thickness was adjusted across four values: 2 mm, 3 mm, 4 mm, and 5 mm, maintaining a constant overall gate thickness of 30 mm. A summary of the various gate configurations is provided in Table 2. The same shell elements and material properties described earlier were utilized, and all gates were subjected to equivalent linear loading until failure. The subsequent sections will detail the effects of varying lattice sizes and dimensions.

Table 2. Different Configurations of Latticed Core Gates

Group	ID	Thickness of Skin Plates (mm)	Core Thickness (mm)	Mass (Kg)
G(1) (Spacing 256 mm)	S1-2/2	2	2	45
	S1-2/3	3		64
	S1-2/4	4		83
	S1-2/5	5		102
	S1-3/2	2	3	48
	S1-3/3	3		66.75
	S1-3/4	4		85.60
	S1-3/5	5		104.44
	S2-2/2	2	2	47.48
	S2-2/3	3		66.35
	S2-2/4	4		85.23

G(2) (Spacing 160 mm)	S2-2/5	5		104.11
	S2-3/2	2		51.69
	S2-3/3	3	3	70.25
	S2-3/4	4		88.80

	S2-3/5	5		107.35
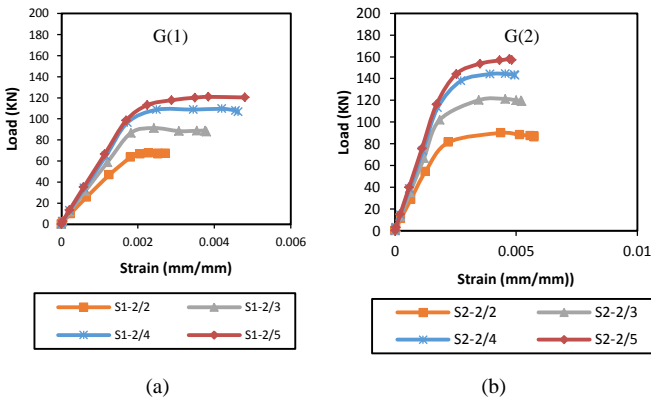
B. Effect of Lattice Core Spacings

The Load-Strain curves obtained from the parametric analysis for the two groups of rhombus lattice structures are presented in Figures 13 and 14. The results indicate that reducing the lattice core's internal spacing enhances both the lattice structures' stiffness and loading capacity when comparing Group 1 (G1) and Group 2 (G2). For G2, the maximum loading capacities for gates with a core size of 2 mm and skin plate thicknesses of 2 mm, 3 mm, 4 mm, and 5 mm were 22%, 26%, 26%, and 24% higher than those of their corresponding G1 gates, respectively. This increase in capacity came with a slight rise in weight, ranging from 1% to 5%, as shown in Figure 15. For a core thickness of 3 mm, gates in Group 2 (G2) demonstrated increased loading capacities of 27%, 23%, 23%, and 17% compared to Group 1 (G1) for skin plate thicknesses of 2 mm, 3 mm, 4 mm, and 5 mm, respectively. This was accompanied by a slight weight increase of 2% to 7%. Overall, reducing the lattice core spacing from one-sixth to one-tenth of the diagonal had a modest impact on load capacity. The average increases in flexural performance were 25% for a core thickness of 2 mm and 23% for a core thickness of 3 mm.

C. Effect of Skin Plate Thickness

Figure 16 shows how increasing the thickness of skin plates affects the latticed systems for Groups 1 (G1) and 2 (G2). For G1 with a 2 mm core thickness, increasing the skin plate from 2 mm to 3 mm, 4 mm, and 5 mm enhanced the capacity by 25%, 37%, and 44%, while the weight increased by 30%, 45%, and 56%, respectively. At a core thickness of 3 mm, the capacity increases were 29%, 41%, and 49%, with corresponding weight increases of 28%, 44%, and 54%.

For G2, at a 2 mm core thickness, the capacity increased by 27%, 40%, and 45% with skin plate thicknesses of 2 mm, 3 mm, 4 mm, and 5 mm, respectively, alongside weight increases of 28%, 44%, and 54%. At a 3 mm core thickness, the capacity increased by 25%, 37%, and 42%, with weight increases of 26%, 41%, and 51%. Thus, increasing skin plate thickness significantly enhances gate load capacity, regardless of lattice core spacing.

(a)   (b)

Figure 13. Load-Strain curves for G(1)& G(2) Models at 2 mm latticed core thickness
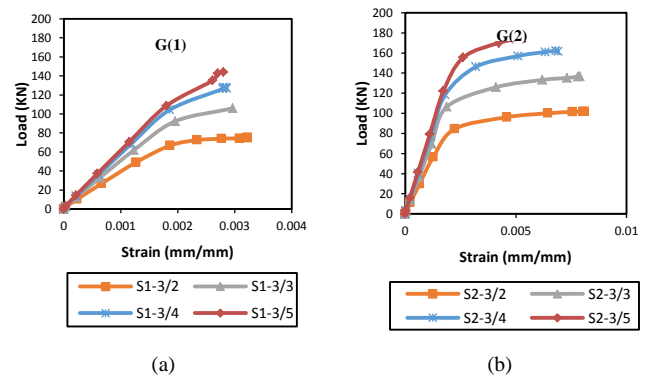

(a)   (b)

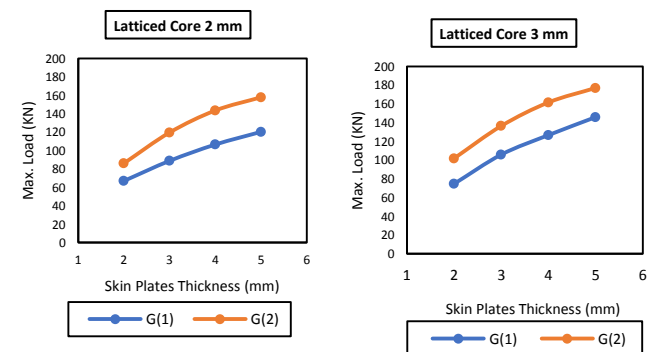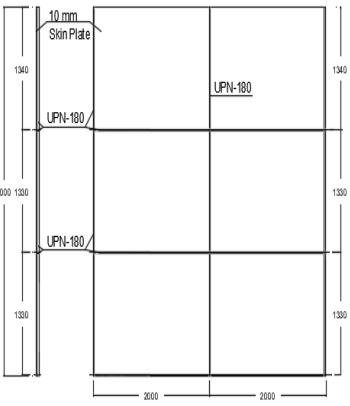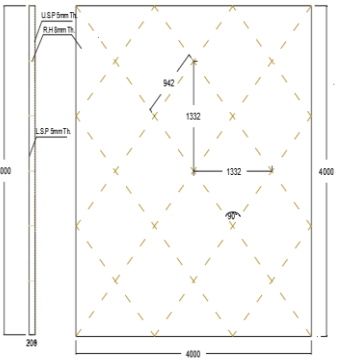**Figure 14. Load-Strain Curves for G(1)& G(2) models at 3 mm latticed core thickness**

Figure 15: Load Capacity of G(1) & G(2) for latticed core thickness: (a) 2 mm, and (b) 3 mm

Table 3. Summary of Large-scale Gates

Proto-type ID	Description	Gates Prototype
B-TG	Typical Gate, Skin plate 6mm with Channels UPN-180 X & edge beams (Mass = 2142 Kg)	
B-LG	Latticed Core Gate (Th. 200 mm) Upper layer (5 mm) –Lower (5mm) ruhmbos Core (8 mm) (Mass = 1674 Kg)	

VII. Practical Application

To evaluate the behavior of full-scale steel gates under normal operational conditions, two gates, each measuring 4000 mm x 4000 mm, were numerically simulated. One gate was designed following conventional methods, while the other utilized a newly proposed latticed gate system.

Conventional Gate (B-TG):

This gate was modeled with a 10 mm thick skin plate on the water-facing side, reinforced by crossbeams (UPN-180) welded at 1330 mm intervals, starting from the bottom edge. The

crossbeams were connected at their ends by two edge beams (UPN-180).

Latticed Gate (B-LG):

This design featured 5 mm thick upper and lower skin plates connected by an internal lattice core, 8 mm thick. The core formed a rhombus pattern with a side length of 942 mm, equivalent to one-sixth of the gate's diagonal. The overall thickness of the latticed gate was 200 mm, as shown in Table 3.

Simulation Details:

Shell elements were used in the numerical model (Figure 17). Both gates were pinned along their vertical edges (Figure 18), and hydrostatic pressure was applied incrementally until failure occurred. The resulting maximum straining stresses were then analyzed.
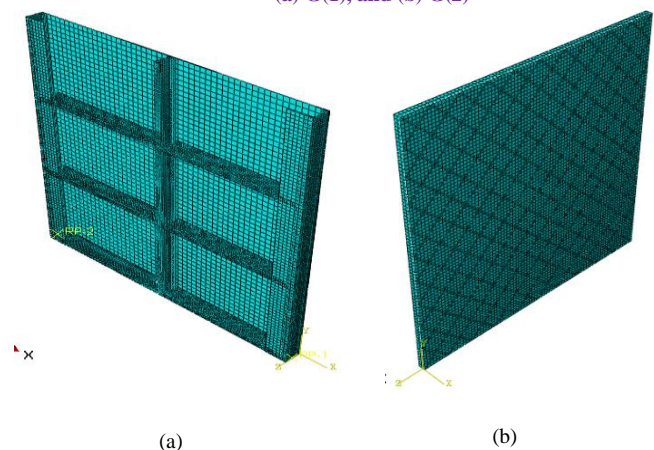

(a)   (b)
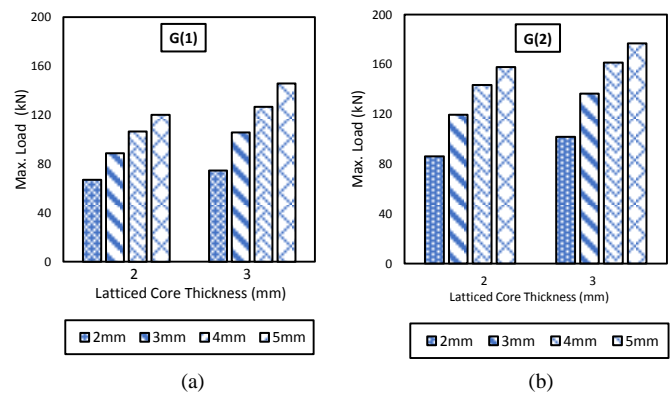
Figure 16. Capacity of gates of different thicknesses of skin plates for (a) G(1), and (b) G(2)

(a)   (b)

Figure 17. Mesh configuration for (a) B-TG and (b) B-LG large-scale gates
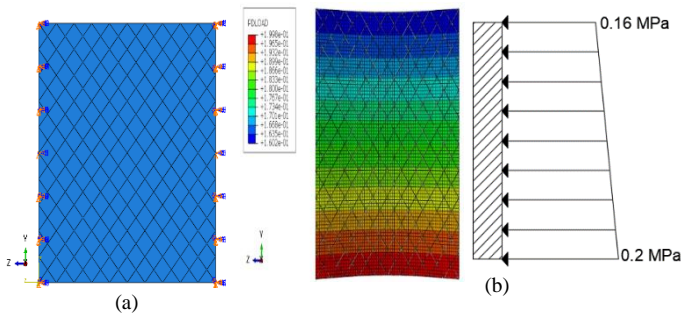
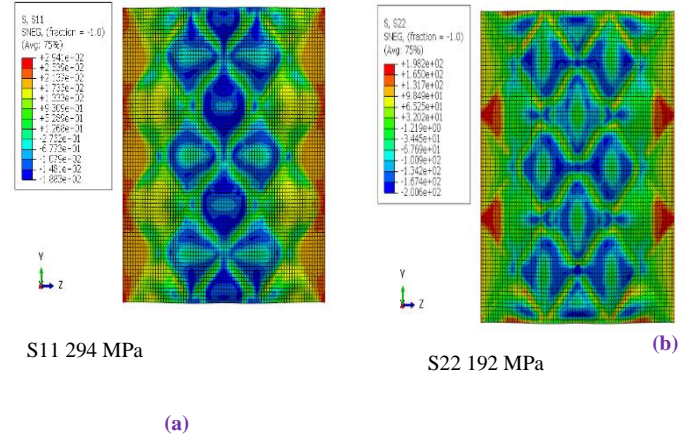**Figure 18. (a) Boundary Conditions, and (b) Typical Load distribution on gates**

A. Large-Scale Gates Results

This section presents the numerical modeling results for the two steel gates. When subjected to a trapezoidal hydrostatic pressure corresponding to a 20-meter water head, both gates reached nearly the maximum allowable stress for steel. Despite this, the deformation patterns for both gates were almost identical, indicating comparable structural integrity in their designs. Figures 19–23 illustrate the behavior of the gates under loading conditions.

Notably, the latticed gate (B-LG) exhibited superior flexural performance compared to the conventional gate (B-TG). This was evident from the stress distribution across the entire surface of B-LG, whereas stress in B-TG was concentrated around the crossbeams. Additionally, B-LG demonstrated a 22% reduction in total mass compared to B-TG.

In conclusion, when compared to conventional hydraulic gate systems, both for small and large-scale applications, the latticed gate system offers improved performance and significant weight reduction. This weight reduction could lead to lower operational

S11 294 MPa   S22 192 MPa

Figure 20. Maximum stresses (a) S11 in X-Direction & S22 in Y-Direction (MPa); for upper skin latticed plate in B-LG

S11 200 MPa   S22 61.2 MPa
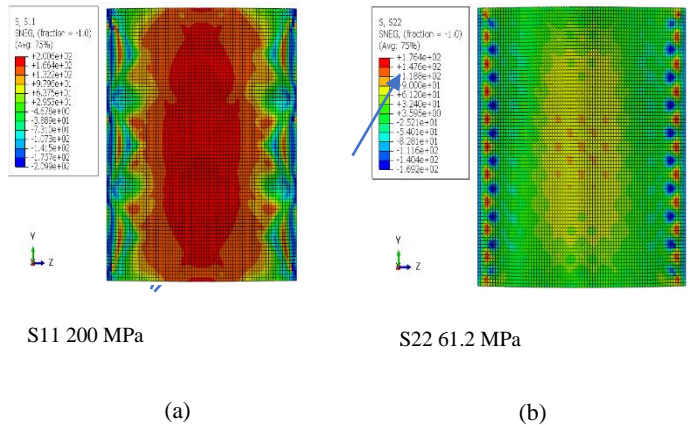
(a)   (b)

Figure 21: Maximum stresses (a) S11 in X-Direction & S22 in Y-Direction (MPa); for lower skin latticed plate in B-LG

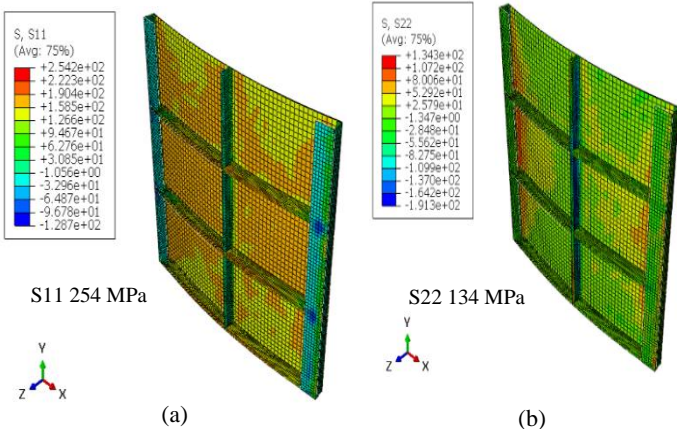
S11 254 MPa   S22 134 MPa

(a)   (b)

Figure 19: Maximum stresses for B-TG (MPa); (a) S11 in X-Direction and (b) S22 in Y- Y-Direction

(a)   (b)

Figure 22: Maximum Deflection (mm) in loading direction; (a) B-TG, and (b) B-LG
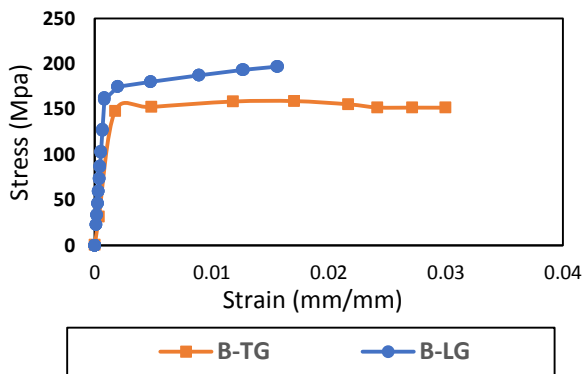
Figure 23. Stress- Starin Curves for large-scale gates

VIII. CONCLUSION

Experimental and numerical studies were conducted on three prototype hydraulic steel gates to evaluate their performance under normal operational loads. The research aimed to introduce a novel latticed core system designed to bear higher loads while reducing the overall gate mass. The key findings of the study are summarized below:

Experimental Results:

The latticed steel gate (LG30) demonstrated the best performance in resisting applied loads, outperforming both the traditional steel gate (TG) and the plain plate gate (PG14). LG30 was 30% lighter than TG, while PG14 was 42% heavier than TG.

Numerical Analysis:

Numerical simulations showed good agreement with the experimental results. When loaded to failure, the latticed gate (LG30-N) exhibited a 14% higher load-carrying capacity compared to the traditional gate (TG-N).

Parametric Study - Core Spacing:

Reducing the core spacing of the latticed gate from one-sixth to one-tenth of the gate's diagonal resulted in a notable increase in load-carrying capacity. The increase was approximately 23% for one-sixth spacing and 25% for one-tenth spacing.

Parametric Study - Skin Plate Thickness:

Increasing the skin plate thickness significantly enhanced the load-carrying capacity. For gate G (1), increasing the skin plate from 2 mm to 5 mm boosted the capacity by 25%-44% for a 2 mm core and by 29%−49% for a 3 mm core. Similarly, for gate G (2), the capacity increased by 27%−45% for a 2 mm core and by 25%−42% for a 3 mm core.

Large-Scale Applications:

The latticed steel system also showed promising results for larger-scale gates. The latticed gate (B-LG) outperformed the traditional gate (B-TG) and achieved a 22% reduction in overall mass.

REFERENCES

[1] P. Examiner and F. L. Lagman, "Irrigation Gate System," U.S. Patent. vol. 2, no. 12, 2006.
[٢] S. K. Pibars, "Design of an on-Farm Irrigation Gate for Lined Lateral Canals 1 Imam," pp. 771–780, 2019.
[٣] P. C.F. Erbisti, "Design of Hydraulic Gates," Taylor & Francis Group, 2014. doi: 10.1201/b16954.
[٤] R. A. Daniel, "Modern solutions for vertical lift gates as closures in locks, river dams, and flood barriers, In ż ynieria Morska i Geotechnika (Maritime and Soil Engineering), no. 2023/04, Gdansk," 2023.
[٥] S.H. Chen, "Hydraulic Steel Gates," Research Gate, 2015, pp. 869–896. doi: 10.1007/978-3-662-47331-3_15.
[٦] USACE, "Design of Hydraulic Steel Structures," 1110-2-584, June, p. 284, 2014.
[٧] N. Jaiswal, "Analysis-and-optimization-of-hydraulic-gate," Research Gate, 2021.
[٨] R. J. Dexter, H. N. Mahmoud, J. A. Padula, and G. A. Riveros, "Fitness-for-Purpose Evaluation of Hydraulic Steel Structures," November, pp. 52–66, 2007.
[٩] R. A. Daniel, "Control of Fatigue in Hydraulic Steel Structures," IABSE Symp. Prague, 2022 Challenges Exist. Oncoming Struct. - Rep., pp. 1234–1241, 2022, doi: 10.2749/prague.2022.1234.
[١٠] X. Q. Liu, L. H. Zhao, H. Y. Cao, and X. P. Sun, "Lifting force acting on a gate with high head," J. Hydrodyn., vol. 23, no. 3, pp. 379–383, 2011, doi: 10.1016/S1001-6058(10)60126-6.
[١١] Y. Lu, Y. Ding, J. Zhang, and M. Yang, "Study on the calculation method of the Honeycomb Steel Structure," Heliyon, vol. 9, no. 5, pp. 139–143, 2023, doi: 10.6919/ICJE.202405.
[١٢] S. Nazeer and S. Allabakshu, "Design and Analysis and of Honeycomb Structures and with Different Cases," Int. J. Eng. Dev. Res., vol. 3, no. 4, pp. 144–156, 2015, [Online]. Available: www.ijedr.org
[١٣] C. Baumgart, C. Weigelt, C. G. Aneziris, and L. Krüger, "Mechanical Properties of High-Density TRIP Steel Honeycomb Structures with Varying Cell Profiles Under Different Loading Conditions," EPJ Web Conf., vol. 183, 2018, doi: 10.1051/epjconf/201818303014.
[١٤] A. Abbadi, Y. Koutsawa, A. Carmasol, S. Belouettar, and Z. Azari, "Experimental and numerical characterization of honeycomb sandwich composite panels," Simul. Model. Pract. Theory, vol. 17, no. 10, pp. 1533–1547, 2009, doi: 10.1016/j.simpat.2009.05.008.
[١٥] V. Matta, J. Suresh Kumar, D. Venkataraviteja, and G. B. K. Reddy, "Flexural Behavior of Aluminum Honeycomb Core Sandwich Structure," IOP Conf. Ser. Mater. Sci. Eng., vol. 197, no. 1, 2017, doi: 10.1088/1757-899X/197/1/012046.
[١٦] E. Sather, "An Analytical Method to Calculate Effective Elastic Properties of General Multifunctional Honeycomb Cores in Sandwich Composites," no. April, 2019, [Online]. Available: http://www.sti.nasa.gov
[١٧] M. T. C. A. D. Cam, "Design and Analysis of Honeycomb Structures," Anveshana's Int. J. Res. Eng. Appl. Sci., vol. 1, no. 12, pp. 111–125, 2016.
[١٨] C. Baumgart, T. Halle, C. Weigelt, L. Krüger, and C. G. Aneziris, "Effect of Honeycomb Cell Geometry on Compressive Properties: Finite Element Analysis and Experimental Verification," Sci. Technol. Mater., vol. 30, no. 1, pp. 35–42, 2018, doi: 10.1016/j.stmat.2018.02.001.
[١٩] G. Camata and P. B. Shing, "Static and Fatigue Load Performance of a GFRP Honeycomb Bridge Deck," Composite. Part B Eng., vol.41, no.4, pp. 299–307, 2010, doi: 10.1016/j.compositesb.2010.02.005.
[٢٠] G. Ghongade, K. P. Kalyan, R. Vaira Vignesh, and M. Govindaraju, "Design, Fabrication, and Analysis of Cost-Effective Steel Honeycomb Structures," vol. 46, pp. 4520–4526, 2019, doi: 10.1016/j.matpr.2020.09.694.
[٢١] A. Javanmardi, K. Ghaedi, Z. Ibrahim, F. Huang, and P. Xu, "Development of a New Hexagonal Honeycomb Steel Damper," Arch. Civ. Mech. Eng., vol. 20, no. 2, 2020, doi: 10.1007/s43452-020-00063-9.

[٢٢] J. Monteiro, "Design and Application of Lattice Structures on Sandwich Panels Core," Inst. Super. Técnico, Univ. Lisbon, Port., November, pp. 1–10, 2019.

[٢٣] Bernardo Capelo Coelho, "Modeling and Characterization of Honeycomb Structures with Density Gradient Produced by Additive Manufacturing Technologies," Univerisdade de Lisboa, November, 2022.

[٢٤] B. Elbably, A. Anwar, H. Altobgy, and G. Elsaeed, "Flexural and Tensile Performance of Laminated GFRP as Suitable Alternative to Hydraulic Steel Gates," JES. J. Eng. Sci., vol. 52, no. 2, 2024, doi: 10.21608/jesaun.2024.243091.1273.

[٢٥] Housing & Building Nat. Research Center, "Egyptian Code of Practice 'Allowable Stress Design,'" no. 279, 2001.

[٢٦] C. A. E. User, "Abaqus theory manual," Abaqus 6.13 Doc., no. Dassault Systems Simulia Corp., Providence, RI, USA., 2014.

[٢٧] I. Faridmehr, M. Hanim Osman, A. Bin Adnan, A. Farokhi Nejad, R. Hodjati, and M. Amin Azimi, "Correlation Between Engineering Stress-Strain and True Stress-Strain Curve," Am. J. Civ. Eng. Archit., vol. 2, no. 1, pp. 53–59, 2014, doi: 10.12691/ajcea-2-1-6.